# Dynamics and rupture of doped Motility Induced Phase Separation

R. Fernández-Quevedo
*Dep. Est. de la Materia, Física Térmica y Electrónica, Universidad Complutense de Madrid, 28040 Madrid, Spain*

E. Chacón
*Instituto de Ciencia de Materiales de Madrid, CSIC, 28049 Madrid, Spain*

P. Tarazona
*Departamento de Física Teórica de la Materia Condensada, Condensed Matter Physics Center (IFIMAC), Universidad Autónoma de Madrid, 28049 Madrid, Spain*

C. Valeriani
*Dep. EMFTEL, Universidad Complutense de Madrid, 28040 Madrid, Spain*
(Dated: May 15, 2025)

## I. THEORETICAL DETAILS

### A. Position of the dense cluster and time average of density profiles

To study the interfacial properties of MIPS formed in an active (A)/passive (P) binary mixture of Brownian particles, we prepare the system in a 2D elongated box (with periodic boundary conditions): this allows the dense/dilute interface to be perpendicular with respect to the long $X$ axis. Passive particles (P) induce motion of the dense active/passive slab. Swift displacements over the periodic simulation box are observed (see snapshots at Fig. 1 in the main text) and we have characterized these fast-moving structures.

A plain time average $\langle ... \rangle_t$, of the density profile,

$$\rho(x) = \left\langle \frac{1}{L_y} \sum_{i=1}^{N} \delta(x - x_i(t)) \right\rangle_t , \tag{1}$$

without taking into account the displacement of the MIPS slab, leads to a trivial flat distribution in the mean density profiles (if averaged over a long time). On the contrary, trying to explicitly maintain the time dependence in the density, by considering the configurations one at the time,

$$\rho(x,t) = \frac{1}{L_y} \sum_{i=1}^{N} \delta(x - x_i(t)), \tag{2}$$

produces too noisy time-dependent density profiles.

To avoid that, we define at each time $t$ a "*slab position*" $X(t)$, as a mesoscopic description of the MIPS structure. Thus, we use $X(t)$ to get shifted mean density profiles

$$\tilde{\rho}(x) = \left\langle \frac{1}{L_y} \sum_{i=1}^{N} \delta(x - x_i(t) + X(t)) \right\rangle_{t \in [t_1, t_2]} , \tag{3}$$

relative to the instantaneous $X(t)$, that would give (non-trivial) long time averages for the particle-level structure of the moving slab.

The main part of the analysis presented in the article concerns the use of such descriptions, averaged over time intervals $[t_1, t_2]$ in which $X(t)$ shows a specific behaviour. Therefore, the definition of $X(t)$ from the instantaneous positions of the particles is an important starting point for our work.

To compute the centre of mass (cm) of the slab, a simple calculation would be

$$X^{cm}(t) \equiv \frac{1}{N} \sum_{i=1}^{N} x_i(t) \equiv \langle x_i(t) \rangle_{[x_0, x_0+L_x]}. \tag{4}$$

where $x_i(t) \in [x_0, x_0 + L_x]$ takes into account the particles' position in a given simulation box (with periodic boundary conditions).

However, different choices for the box (i.e. for $x_0$) lead to different values for $X^{cm}(t)$, since there is not a well defined "centre of mass" for a periodic train of dense slabs separated by less dense regions. The problem may be solved by imposing that, at each time, the value of $x_0(t)$ is taken to minimize the second moment of the density distribution $I(t) = \sum_j (x_j(t) - X(t))^2$. However, this variational definition is computationally expensive and produces some (weak but troublesome) lost of periodicity in the relative density profile $\tilde{\rho}(x)$. This problem may be solved with a smooth weight local average, rather than the sharp boundaries $x_0 \le x_i < x_o + L_x$ used in Eq. (4).

However, we hereby present a more convenient alternative, defining $X(t)$ (see Eq. (4) of the main text) to get a real positive value for the relative particle positions Fourier component

$$\hat{\rho}(q_1, t) = \sum_{j=1}^{N} e^{iq_1(x_j(t) - X(t))} \tag{5}$$

with first wavevector ($q_1 = 2\pi/L_x$) in the periodic simulation box.

Along our simulations, these different definitions for the nominal "position of the slab" give very similar results whenever MIPS produces well separated regions with low and high densities. Fig. 1 shows $X^{cm}(t)$ and $X(t)$ over a short simulation for $\eta_P = 0.4$, to show that most of the time these two definitions give very similar results. It is only when the structure experiences strong fluctuations, that creates a rapid change in the structure of the dense slab, that the two definitions for its nominal position may differ. In particular $X^{cm}(t)$ may become discontinuous, since the variational definition for the second moment may jump between two values of $x_o(t)$ that are local minima for $I(t)$. In contrast, the Fourier component definition Eq.(5) gives always a continuous evolution for $X(t)$, even if it has very rapid movements reflecting a reorganization of the slab structure.

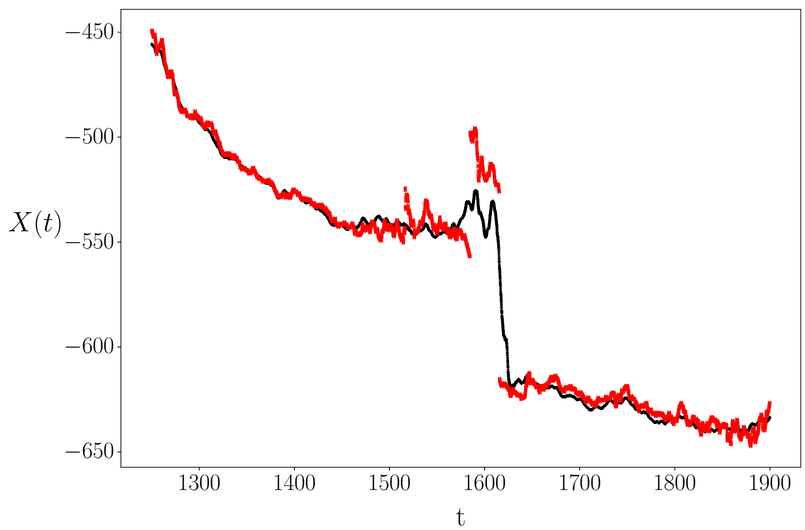


FIG. 1. Comparative of different definitions for the position of the dense MIPS slab, over a short part of the simulation for $\eta_P = 0.4$. The black line is the Fourier definition, $X(t)$ in Eq. (5), and the red line is the centre of mass definition, $X^{cm}(t)$ (4) with the requirement of minimum second moment.

Thus, in all the results presented in the main article and here we use the Fourier component definition for $X(t)$, as the optimal separation between the mesoscopic "position of the MIPS slab", $X(t)$, and the "molecular description" given by the density distribution $\tilde{\rho}(x)$, calculated from the particles distances to that $X(t)$.

It is important to realize that $V(t)$ obtained from the change of $X(t)$ between time steps (see Eq.(5) of the main text), should be called "apparent velocity" of the MIPS structure, because it is not directly related to the mean (or centre of mass) instantaneous velocity of the particles,

$$v_\alpha^{cm}(t) \equiv \frac{1}{N} \sum_{i_\alpha=1}^{N_\alpha} v_i^\alpha(t) \tag{6}$$

for each species ($\alpha = A, P$). $v_\alpha^{cm}(t)$ is well defined (it is the same for any choice of $x_0$ in Eq. (4), so that the second moment condition for $X^{cm}(t)$ may be waived). However, as discussed in the main text, that centre of mass velocity can be different for each component ($\alpha$), and none equal to the apparent velocity of the slab $V(t)$. The equality $v^A(t) = v^P(t) = V(t)$ would imply a rigid displacement of the density profiles, which could result from the fact that (on average) the velocities of the particles are the same, regardless of their position $x$, but that is an impossible steady state under the hypothesis of the Brownian Dynamics and the uncorrelated fluctuations of the active forces. Any steady state displacement of the slab position $X(t)$ has to be related to local variations in the mean velocity of the particles, so that the displacement of $\rho_\alpha(x,t)$ implies some kind of "*sink/source*" effects, in which the particles join the dense cluster at one interface and leave it at the other side. Thus, the slab could seem to move even if the particles at its centre had zero mean velocity [4]. In section I.B below we present some detailed analysis of this dynamics.

### B. Velocity auto-correlation and time scale separation

In order to characterize the separation of time scales, we identify the SMPs along the simulations for each $\eta_P$, as shown in Fig. 2 of the main text, and calculate over them the velocity autocorrelation

$$C(t) = \langle (V(t_0) - \langle V\rangle)\,(V(t_0+t) - \langle V\rangle)\rangle_{t_0} \approx \left\langle (V(t) - \langle V\rangle)^2 \right\rangle_t e^{-\dfrac{t}{\tau_p}}, \tag{7}$$

where $\langle V\rangle$ is the mean velocity (over that SMP), $V(t)$ is the instantaneous velocity, calculated using Eq. (5) of the main text, and $t_0$ the initial time over which we average. The persistence time, $\tau_p$, in the expected exponential decay of $C(t)$, represents the typical time in which the slab loses memory of the fast fluctuations of its structure, but keeping the persistent and global characteristics that produce the (apparent) steady motion over the SMP. Therefore, the characterization of these structures through $\tilde{\rho}(x)$ in Eq. (3) should be robust only with time averages much larger than $\tau_p$.

Fig. 2 shows (in black) the results for several time intervals of the simulation, with a total duration of $\Delta t = 250$. The red lines represent the exponential fits of the data to Eq. 7, which allows us to determine the persistence time for each $\eta_P$. For Both the purely active system and all the binary mixtures we find similar persistence times $\tau_p \approx 1.8 \pm 0.2$, and also similar mean square fluctuations $\Delta V = \langle (V(t) - \langle V\rangle)^2\rangle^{1/2} \approx 0.6$, from the value $C(0)$.

In the pure active system ($\eta_P = 0$, blue line in Fig. 2(a) of the main text), the slab position $X(t)$ follows a pure random walk for any time much larger than $\tau_p$, without any other relevant time scale. In contrast for $\eta_P = 0.4$ (black line in Fig. 2(d) of the main text) we observe very long SMPs, over a time scale $\tau_{SMP} > 1000$, in which $V(t)$ fluctuates around a well defined mean value $\pm V_{SMP}$, with $V_{SMP} \approx 0.57 \pm 2$. Similar behaviour, although with shorter SMPs and lower $V_{SMP}(\eta_P)$ is observed for $\eta_P = 0.3$ ($V_{SMP} \approx 0.36 \pm 2$ and $\tau_{SMP} \sim 1000$, Fig. 2(c) of the main text) and $\eta_P = 0.2$ ($V_{SMP} \approx 0.30 \pm 3$ and $\tau_{SMP} \sim 500$, Fig. 2(b) of the main text). The SMPs are interrupted by sharp changes in $X(t)$ that indicate a large fluctuation in the structure of the MIPS slab, leading to periods in which $X(t)$ fluctuates around a constant value.

We may estimate that for $\eta_P = 0.4$ there is a typical time $\tau_o \sim 100$ (just in order of magnitude) between two SMPs, in which $|\langle V(t)\rangle| \ll V_{SMP}$. Therefore, for that high concentration of passive particles $\tau_p \ll \tau_o \ll \tau_{SMP}$ gives a good separation of time scales for our analysis of SMPs. For lower $\eta_P$, $\tau_o$ increases while $\tau_{SMP}$ decreases, so that for $\eta_P = 0.2$ we may estimate $\tau_o \sim \tau_{SMP} \sim 500$. The simulation for $\eta_P = 0.1$ shows a $X(t)$ with evident differences with respect to the pure random walk at $\eta_P = 0$; however, $\tau_{SMP} < \tau_o$ and the low value of $V_{SMP}$ make unclear the separation of the trajectories $X(t)$ in the SMPs and the intervals between them. Notice that we have only crude estimations for $\tau_{SMP}(\eta_P)$ and $\tau_o(\eta_P)$, since good statistics would require extremely long simulation runs.

Thus, our results give a clear account on how a large enough concentration of passive particles creates a qualitative difference with the pure ABP system.

### C. Probability distribution for the velocity

Figure (3) presents, for $\eta_P = 0.2$, the separation of the band trajectories $X(t)$, the instantaneous velocities $V(t)$, and their histograms, separated (by colour) in the SMP periods with $\langle V(t)\rangle = V_{SMP}$ (red), $-V_{SMP}$ (blue), and in the intervals with $\langle V(t)\rangle \approx 0$ between them (green). The rapid (time scale $\tau_p = 1.8$) fluctuations of the instantaneous velocity have a standard deviation of $\Delta V \approx \pm 0.54$, larger than the mean values $\langle V(t)\rangle = \pm V_{SMP}(\eta_P) \approx 0.30$ in the SMPs, so that without a decomposition of the trajectories $X(t)$ in the $\sim \tau_{SMP}$ and $\sim \tau_o$ long intervals the histogram for $V(t)$ could be taken as a (slightly broader, $\Delta V \approx \pm 0.65$) single Gaussian peak, with $\langle v(t)\rangle \approx 0$. For $\eta_P = 0.2$, our simulation run is long enough (compared with $\tau_{SMP}$) to get not far from a balance between the forth and back

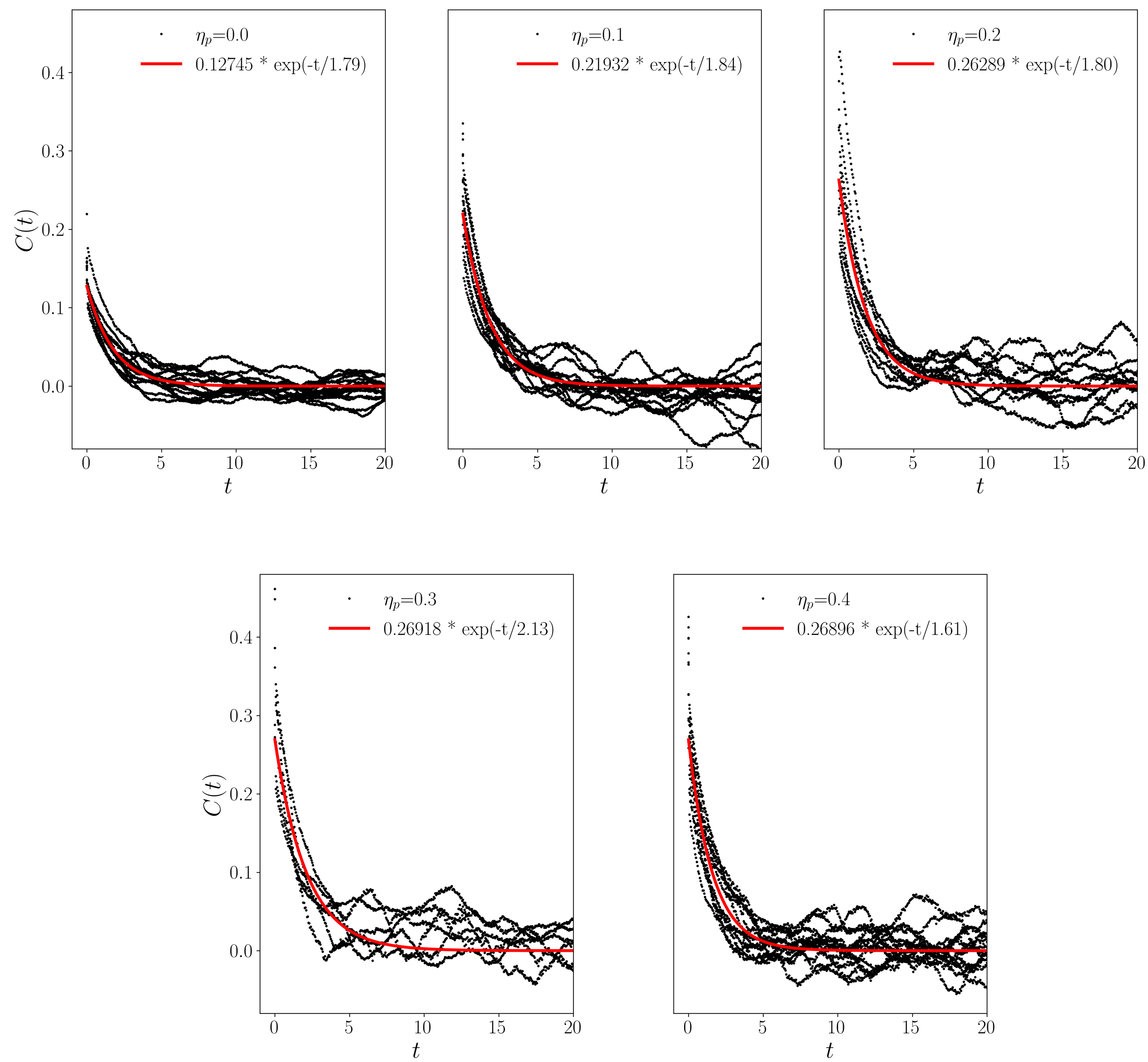


FIG. 2. Black dots at each panel: Velocity autocorrelation of the dense MIPS band (Eq. 7) for different values of $\eta_p$, calculated over several ranges of $\Delta t = 250$ selected within SMPs. The corresponding fits (red lines) to the exponential decay, Eq. 7 give the persistence time $\tau_p$.

SMPs, that together amount about 46% of the trajectory time, with about 54% left for the time intervals in which the fluctuations of $X(t)$ show no bias.

For $\eta_P = 0.4$, in Figure (4) the similar separation gives that forwards (68%) and backwards (29%) SMPs take most the trajectory, with just a short (3%) interval for a U-turn between them. The histograms over the SMP, with standard deviation $\Delta V \approx 0.6$ over the mean values $\langle(V(t)\rangle \approx \pm 0.57$, show the increase of $V_{SMP}(\eta_P)$ with $\eta_P$, with no significative change the rapid ($\sim \tau_p$) fluctuations. In this case, our simulation is obviously too short to get a good statistical sampling of the SMPs, with results in a clear asymmetry in the velocity histogram if taken over the full simulation.

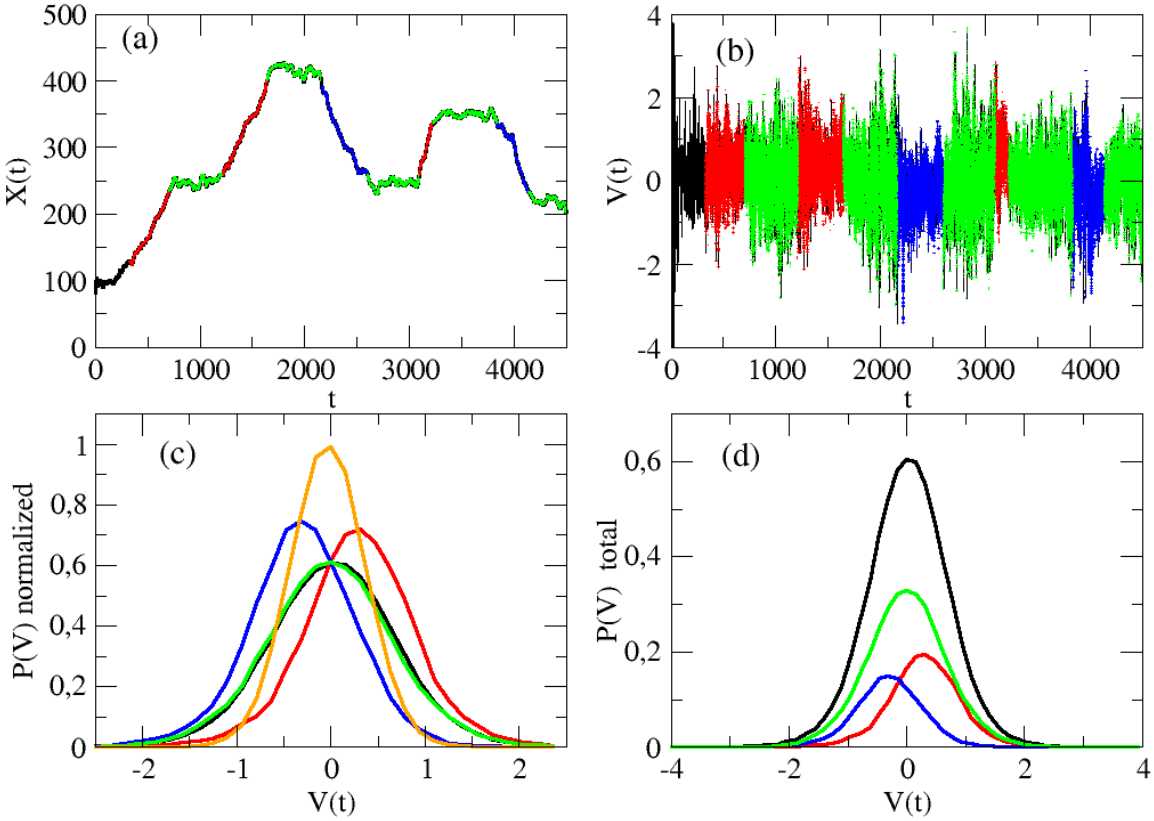


FIG. 3. For the $\eta_P = 0.2$ system, the trajectory of the MIPS slab $X(t)$ (a) and its velocity $V(t)$ (b) are presented in different colours: red for the SMP with $V(t) \approx 0.3$, blue for the SMP with $V(t) \approx -0.30$, and green for the periods in which $X(t)$ remains approximately constant (on a time scale $t \gg \tau_p$); a initial period for equilibration (in black) is leave out of the analysis. (c) Normalized histograms for $V(t)$ over each fraction of the trajectory (with the same colour code, red,blue and green), the black line is the normalized histogram over the entire trajectory and the orange line the same histogram for the pure ($\eta_P = 0$) system of ABP. (d) The velocity histograms for $\eta_P = 0.2$ are presented but normalized now to the full (black line), to show the relative weight of each kind of movement along the simulation.

### D. Analysis of steady flow states

As the passive particle concentration, $\eta_P$, increases the steady motion periods (SMPs) are longer and, therefore, for high $\eta_P$ the MIPS slabs keep moving in the same direction during long simulation times with a well defined mean velocity $\langle V(t)\rangle = V$, from Eq.(5) of the main text. The density profiles, relative to the instantaneous $X(t)$, Eq.(3), may be averaged over many configurations and they show a clear asymmetry already proven at reference [4], being much sharper at the receding edge that at the advancing one, showing also qualitative difference between active ($A$) and passive ($P$) particles. The former have enhanced relative concentration at the advancing front and strongly deplected at the receding one.

Since these structures travel in the same direction for long simulation times, their density profiles may be analysed as steady state structures. Following a similar approach to the one found in the reference [5], under the assumption that a time dependent density profile $\rho(x,t)$, much better averaged that in Eq.(2), may be represented by $\rho(x,t) = \tilde{\rho}(x - Vt)$. The continuity equation for each specie is

$$\partial_t \rho_\alpha(x,t) = -\partial_x j_\alpha(x,t) \tag{8}$$

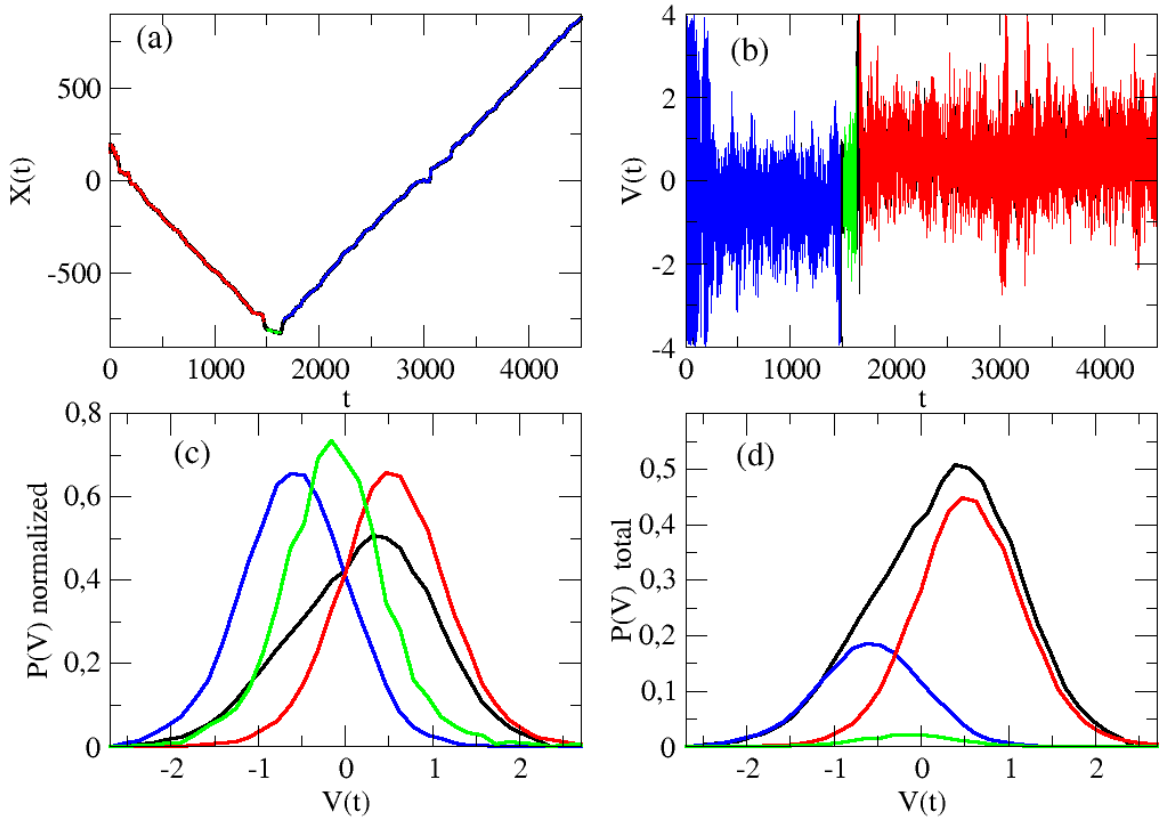


FIG. 4. As in Fig. (3) but for $\eta_P = 0.4$. The longer typical time of the SMPs, $\tau_{SMP}$, makes the simulation trajectory obviously too short to sample the back and forth alternation of the SMPs, but the statistical distribution for $V(t)$ is very similar to the $\eta_P = 0.2$ case, just with a larger separation between the red and blue peaks. The time $\tau_{SMP}$ being comparable to the total simulation time, in this case panel (d) shows quite unbalanced statistical weights for forward (red) and backwards (blue) motion.

being $\alpha = A, P$. This equation relates the density profiles $\rho_\alpha(x,t) \equiv \rho_\alpha(x - Vt)$ with the current (in X direction) $j_\alpha(x,t) \equiv j_\alpha(x - Vt)$. Since the velocity is constant along the SMP it must be fulfilled that

$$\partial_t \rho_\alpha(x,t) = -V \partial_x \rho_\alpha(x,t) = -\partial_x j_\alpha(x,t) \tag{9}$$

Thus, integrating the previous differential equation, a generic expression for the current density of the particles is

$$j_\alpha(x,t) = V \rho_\alpha(x - Vt) + \Delta_\alpha \tag{10}$$

with $\Delta_\alpha$ positive uniform counter-current, which allow to distinguish between the apparent velocity of the slab, $V$, and the mass centre velocity of each specie, which may be defined as

$$\langle v_\alpha \rangle \equiv \frac{1}{N_\alpha} \left\langle \sum_{j=1}^{N_\alpha} v_i \right\rangle = \frac{\int_0^{L_x} dx j_\alpha(x,t)}{\int_0^{L_x} dx \rho_\alpha(x,t)} - \Delta_\alpha = \langle V \rangle - \frac{\Delta_\alpha}{\langle \rho_\alpha \rangle} \tag{11}$$

From the Eq. 10, the counter-current may be calculated as

$$\Delta_\alpha = V \rho_\alpha(x - Vt) - j_\alpha(x - Vt) \tag{12}$$

Since the system has Brownian dynamics, the velocities are proportionals, via the $\Gamma$ constant, to the total instantaneous force over each particle, $v_i(t) = \Gamma F_i(t)$, and, therefore, the currents of $P$ and $A$ particles are proportional to the force densities, $j(x,t) = \Gamma f(x,t)$. Thus,

$$j_\alpha(\hat{x}) = \Gamma \left( kT \frac{\partial \tilde{\rho}_\alpha}{\partial \tilde{x}}(\hat{x}) + \sum_{\beta=A,P} f_{\alpha,\beta}(\hat{x}) + f^a(\hat{x}) \right) \tag{13}$$

with the thermal Brownian noise effect through the density gradient $(kT\, \partial_x \rho_\alpha(x,t))$, the components $f_{\alpha,\beta}$ for the interaction force produced by particles $\beta$ upon particles $\alpha$, and the active force density $f^a$ (zero for the passive particles); all them in terms of the steady running coordinate $\tilde{x} = x - \langle V \rangle t$.

Thus, joining the Eq. 12 and Eq. 13 we get:

$$\Delta_\alpha = V \rho_\alpha(\tilde{x}) - \Gamma \left( kT \frac{\partial \rho_\alpha(\tilde{x})}{\partial x} + \sum_{\beta=A,P} f_{\alpha,\beta}(\tilde{x}) + f^a(\tilde{x}) \right) \tag{14}$$

Since there is no correlation between the directions of active forces for different particles, averaging the active force over the entire simulation box yields to

$$\frac{1}{L_x} \int_0^{L_x} dx f^a(t) \approx 0 \tag{15}$$

where $A = L_x L_y$ is the area of the simulation box. The interaction forces between particles of the same species ($f_{AA}$ and $f_{PP}$) cancel each other out. However, an approximately constant net force remains due to the cross interactions between active and passive particles ($f_{AP}$), therefore,

$$\frac{1}{L_x} \int_0^{L_x} dx f_{PA}(t) = -\frac{1}{L_x} \int_0^{L_x} dx f_{AP}(t) \equiv \frac{F_{PA}}{A} = -\frac{F_{AP}}{A}, \tag{16}$$

with the area $A = L_x L_y$ and the global densities $\langle \rho_\alpha \rangle = N_\alpha / A$, we obtain

$$\Delta_\alpha = V \langle \rho_\alpha \rangle - \Gamma \frac{F_{PA}}{A} = (V - \langle v_\alpha \rangle) \langle \rho_\alpha \rangle \tag{17}$$

So, the time average for the mass centre velocity of the passive is given by

$$\langle v_P \rangle \equiv \langle v_P^{cm}(t) \rangle_t = \Gamma \frac{F_{PA}}{A \langle \rho_P \rangle} = \Gamma \frac{F_{PA}}{N_P} \tag{18}$$

and using the same procedure, the time average for the mass centre velocity for the active particles is

$$\langle v_A \rangle \equiv \langle v_A^{cm}(t) \rangle_t = -\Gamma \frac{F_{PA}}{A \langle \rho_A \rangle} = -\Gamma \frac{F_{PA}}{N_A} \tag{19}$$

Therefore, the qualitative role of the passive particles in their mixture with ABP is evident, since in a pure $\eta_P = 0$ system $F_{PA} = 0$ and the (all active) particles have no mean velocity, and Eq.(17) has $\Delta_A = V = 0$ as the only solution, unless we add some external force that breaks the $\pm x$ symmetry.

## II. SOURCE/SINK EFFECT

The proposal to explain the band displacement by Wysocki and coworkers [4] is a source/sink effect, in such a way that the receding interface evaporates particles to the dilute phase constantly, behaving like a source, whereas the advancing front captures particles from the dilute phase into the dense phase, acting as a sink. In the main text we

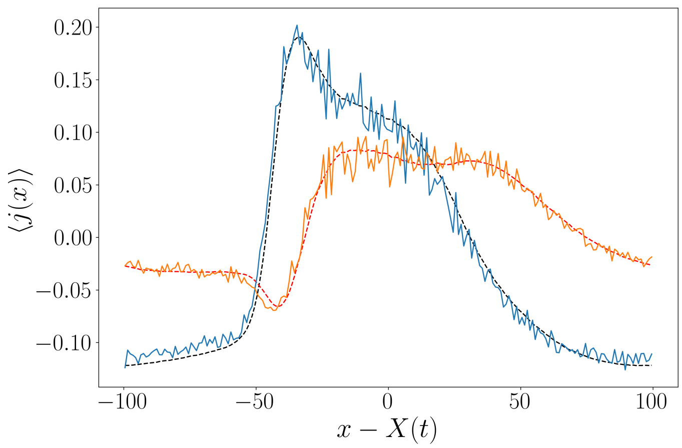


FIG. 5. The current profiles ($j_A(\tilde{x})$ and $j_P(\tilde{x})$) obtained from the simulations with $\eta_P = 0.4$ and $\langle V(t) \rangle = +V_{SMP} = 0.57$. Both sets of profiles are shown: those computed directly from the forces (solid lines, with orange representing passive particles and blue representing active particles) and those derived from the densities (dashed lines, with red for passive particles and black for active particles). Blue and red lines represent the profiles for passive and active particles, respectively. For the same simulation, the velocity profiles derived from theses current profiles are showed in Fig. 7 of the main text.

point that our quantitative analysis shows that the source/sink effect runs in parallel with an actual drift of the dense slab.

Figure 5 presents the current profiles $j_A(\tilde{x})$ and $j_P(\tilde{x})$ sampled in our simulation for $\eta_P = 0.4$, along a SMP period with $\langle V(t) \rangle = +V_{SMP} = 0.57$. The values of the current for each species may be obtained directly from the net force acting on each particle, plus the contribution $-kT\delta_x \rho_\alpha(x)$. For the $\eta_P = 0.4$ mixture the real velocity of the particles at the inner part of the dense slab it that is approximately one third of the apparent velocity $V(t) = dX(t)/dt$, while the other two thirds of $V(t)$ come from the particles in the low density region moving in the opposite direction, out of the source at the back edge and into the sink of the front edge of the slab.

This effect is illustrated in Figure 6 by a sequence of snapshots (time running from top to bottom) for the system with $\eta_P = 0.4$, along the SMP with positive (apparent) velocity of the MIPS slab position $X(t)$, marked by the vertical dashed lines. The wavy full lines give the fluctuating borders of the slab, defined by a Gaussian smoothing of the instantaneous density.

Figure 6-a) (as in Fig. 5 of the main text) represents the complete system, without distinction between the active and passive particles. Here, in order to look at their different behaviours, we present in 6-b) only the active particles and in 6-c) the passive particles.

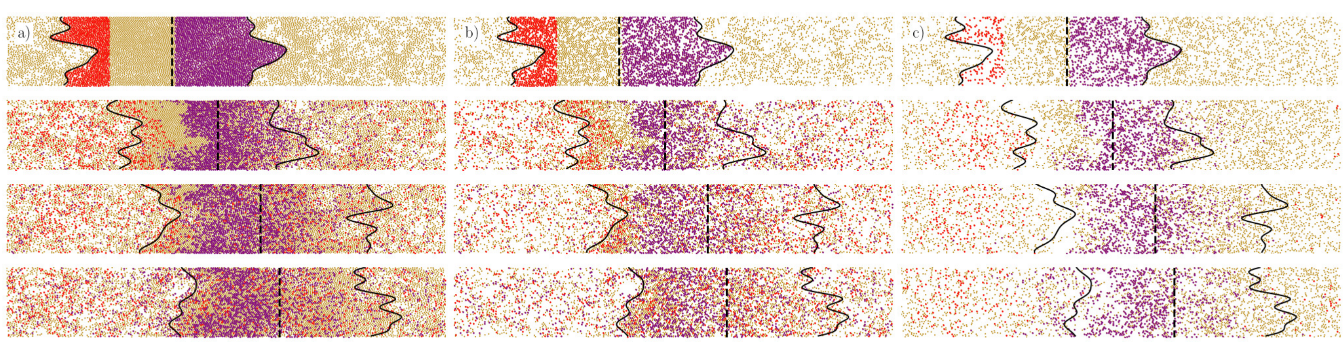


FIG. 6. Snapshots showing the movement of the slab with time (time evolving from top to bottom) for the complete system ($a$ panel), only the active particles ($b$ panel) and the passive particles ($c$ panel). Top snapshot: slab boundaries are underlined in black (line); slab particles on each side are coloured, in cyan (source surface) and purple (sink surface). Their colour is maintained in the following snapshots showing their change of position with time, while the underline slab boundaries changes for each time.

For the three panels in Fig. 6, the particles that in the initial time (top snapshots) are in the dense MIPS cluster and close to one of its interfaces are coloured, red for the source-back interface and purple for the sink-front one. The colour of each particle is maintained in the following snapshots, with time running from top to bottom.

In the 6-a) as time goes on the purple particles move slowly towards the inside of the band, whereas the red ones scape quickly from the back interface to the dilute phase and they are added to the front interface. Nonetheless, the behaviour of active and passive cannot be the same, as our results support. In fact, their mean velocities, $\langle v_A \rangle \approx -0.034$ and $\langle v_P \rangle \approx 0.051$, have different signs, as required by the requirement $N_A \langle v_A \rangle + N_P \langle v_P \rangle = 0.$ by the analysis in Section I D. Those velocities are much lower in absolute value than the (apparent) velocity of the slab $V_{SMP} \approx 0.57$. Therefore, the main effect observed in the time evolution (from top to bottom) for particles with a given colour is that they are dispersed and mixed with those of the neighbour bands colour, with much less global displacement than the position of the slab $X(t)$. In this dispersion, the active particles (central column, panel b) are clearly faster than the passive particles (right side column, panel c), since the (random) active force produces a large enhancement over the diffusion by the thermal noise.

At the central column (active particles, panel b) those at the rear of the MIPS band (in red) diffuse very rapidly towards the left, into the low density region, so that even at the second (from top) frame many of them have gone across the periodic boundary and are already entering into the slab from the right, just a small fraction is drawn forward by the advancing front. Those are the active particles that happen to have their active force in a $n_{i,x} < 0$ direction and move rapidly away from the slab. In the later snapshots, these red-labelled particles are fully dispersed all over the system. Those red-labelled particles at the with $n_{i,x} < 0$, pushing toward the dense slab, have a much more slow diffusion because the molecular collisions transfer the effects of the active force on those particles into a global forward push to the whole slab.

Still looking at the active particles, but now to those (purple coloured) at the left side of the dense region, the active particles at the middle of the slab have even lower diffusion towards the left, which makes visible that they are actually moving (in average) towards the right, although not at fast as the vertical dashed line that marks the nominal position $X(t)$ that we use to describe the position of the slab.

Meanwhile, the passive particles exhibit minimal diffusion. In the final snapshot of 6-c), the positions of the purple particles do not show significant difference compared to the initial snapshot. At the front interface, the behaviour of both active and passive particles is similar, where the diffusion of active particles being notably lower than at the back interface.

The distinct behaviour of the active particles at the two interfaces, influenced by the presence of passive particles, results in a non-zero average velocity for the active particles. The role of the passive particles in the steady displacement of the band is clearly passive, as they exhibit no significant variation in diffusion across the band. However, passive particles introduce the asymmetry between the interfaces, as evidenced in Figure 6-c, where a minimum concentration of passive particles is observed at the back interface, coinciding with the accumulation of active particles, which push the passive in the band movement direction.

The asymmetry in the diffusion of active particles and the depletion of passive particles at the back interface is also reflected in the definition of the interfaces. This is highlighted in Figure 6, where the 'intrinsic' band interfaces, calculated as described in reference [6], are outlined in black. The front interface is smoother in comparison to the back interface. The front primarily consists of passive particles that are captured and dragged along by the movement of the band, alongside active particles propelled by their active force. In contrast, the back interface more closely resembles a typical MIPS interface, where the intrinsic interface is well-defined and follows the fluctuations of the boundary.

## III. COMPLEMENTARY VIDEOS

**Vid_SP_mov_MIX_00.mp4:** Video of the purely active MIPS band running for a total time of $t = 500$.

**Vid_SP_mov_MIX_04.mp4:** Video of an active/passive binary mixture with MIPS band running for a total time of $t = 500$. $\eta_P = 0.4$, the active particles are represented in red and the passive particles in blue.

**Vid_SP_U-turn_v2.mp4:** Animation representing the position of the slab when performing an U-turn. The top panel corresponds to the top panel of figure 9 in the main text, where an arrow points to the position of the slab along the video. The bottom panel represents the configuration corresponding to the time and position of the slab indicated by the arrow (active particles are coloured red, and passive particles are coloured blue, respectively).

[1] A. P. Thompson, H. M. Aktulga, R. Berger, D. S. Bolintineanu, W. M. Brown, P. S. Crozier, P. J. in 't Veld, A. Kohlmeyer, S. G. Moore, T. D. Nguyen, R. Shan, M. J. Stevens, J. Tranchida, C. Trott, and S. J. Plimpton, Comp. Phys. Comm. **271**, 108171 (2022).

[2] J. D. Weeks, D. Chandler, and H. C. Andersen, Role of repulsive forces in determining the equilibrium structure of simple liquids, The Journal of Chemical Physics **54**, 5237 (1971), https://pubs.aip.org/aip/jcp/article-pdf/54/12/5237/18874636/5237_1_online.pdf.
[3] J. Stenhammar, R. Wittkowski, D. Marenduzzo, and M. E. Cates, Activity-induced phase separation and self-assembly in mixtures of active and passive particles, Phys. Rev. Lett. **114**, 018301 (2015).
[4] A. Wysocki, R. G. Winkler, and G. Gompper, New Journal of Physics **18**, 123030 (2016).
[5] F. Penna and P. Tarazona, The Journal of Chemical Physics **119**, 1766 (2003).
[6] E. Chacon, F. Alarcon, J. Ramírez, P. Tarazona, and C. Valeriani, Soft Matter **18**, 2646 (2022).